*ENGINEERING TRANSACTIONS* • *Engng. Trans.* • **64**, 2, 213–223, 2016
Polish Academy of Sciences • Institute of Fundamental Technological Research (IPPT PAN)
National Engineering School of Metz (ENIM) • Poznan University of Technology

# Theoretical and Numerical Study of the Flexural Behaviour of BFRP RC Beams

Dawid PAWŁOWSKI, Maciej SZUMIGAŁA

*Poznań University of Technology*
*Institute of Structural Engineering*
Piotrowo 5, 60-965 Poznań, Poland
e-mail: dawid.p.pawlowski@doctorate.put.poznan.pl

Fiber-reinforced polymer (FRP) bars are a relatively new reinforcement material used in civil engineering. This type of reinforcement has low modulus of elasticity and high tensile strength. Hence, the behaviour of FRP reinforced concrete (RC) members is significantly different to that of traditional steel RC. This paper presents the results of numerical and theoretical studies of the flexural behaviour of simply supported basalt fiber-reinforced polymer (BFRP) RC beams under short-term static loads. The numerical analysis was performed using the finite element method (FEM). The main goal of this paper was to investigate deflections and failure mechanisms of BFRP RC members depending on the reinforcement ratio. The results of the numerical analysis were examined and compared with code formulations.

**Key words:** FEM analysis, composite materials, BFRP reinforcement, BFRP RC beams.

## 1. Introduction

Basalt fiber-reinforced polymer (BFRP) bars are a new material which can be a good alternative to traditional steel for reinforced concrete structures. This type of reinforcement exhibits properties such as corrosion resistance, electromagnetic neutrality and high cuttability [1]. Consequently, it has many applications in structures (e.g., offshore structures, bridges) used in aggressive environments, in structures where electromagnetic neutrality is needed or in temporary structures [2].

BFRP bars have low modulus of elasticity, low shear strength and high tensile strength [3, 4]. Moreover, they do not exhibit any yielding before failure and behave almost linearly up to tensile rupture. Due to their mechanical properties, deflections and cracking in FRP RC flexural members are larger than the ones

found in traditional RC members. As a result, the design of FRP RC beams is often governed by the serviceability limit states [5, 6].

This paper presents the results of a numerical study in which six BFRP RC beams and three steel RC beams were tested in four-point bending. The aim of this simulation was to examine the failure mechanism and deflections of simply supported BFRP RC beams depending on the reinforcement ratio. The results of the numerical simulation were compared with code formulations [3, 7] and with the behaviour of traditional steel RC beams.

## 2. Numerical simulation programme

### *2.1. Test specimens*

Figure 1 presents the geometry and the reinforcement of considered beams.

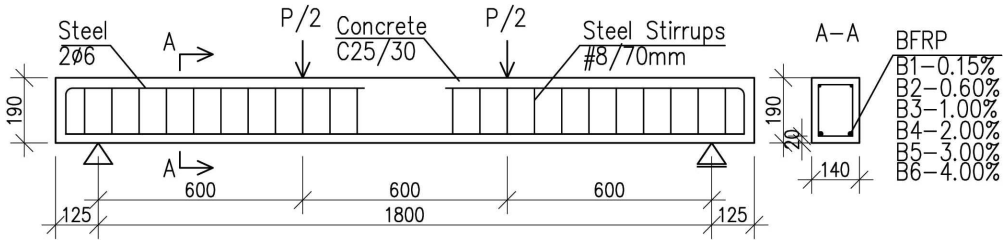


Fig. 1. Geometry and reinforcement of specimen (dimensions in mm).

The numerical study consisted of investigating the flexural behaviour of six beams with varying BFRP reinforcement (Table 1). All the beams had a cross-section of $0.14 \times 0.19$ m$^2$, a total length of 2.05 m and a span of 1.80 m. The shear reinforcement consisted of 8 mm round steel stirrups placed at intervals of 70 mm. In the pure bending zone no stirrups were provided. Two 6 mm steel bars were used as top reinforcement to hold the stirrups.

**Table 1**. Characteristics of specimens.

| Beam Designation | B1 | B2 | B3 | B4 | B5 | B6 |
|---|---|---|---|---|---|---|
| Reinforcement Ratio $\rho_f$ [%] | 0.15 | 0.60 | 1.00 | 2.00 | 3.0 | 4.00 |

### *2.2. Material properties*

*2.2.1. Concrete.* All the beams had a target concrete compressive strength of C25/30 MPa [7]. The properties of concrete are presented in Table 2.

**Table 2**. Mechanical properties of concrete*.

| Modulus of elasticity $E_c$ [GPa] | Compressive strength $f_c$ [MPa] | Tensile strength $f_{ct}$ [MPa] |
|---|---|---|
| 31.0 | 33.0 | 2.6 |

* According to formulas in EN-206:2013 [8].

*2.2.2. BFRP reinforcement.* BFRP ribbed bars were used as the flexural reinforcement. The experimentally determined mechanical properties of reinforcement [4] are shown in Table 3.

**Table 3**. Mechanical properties of BFRP reinforcement.

| Diameter [mm] | Tensile strength $f_{fu}$ [MPa] | Modulus of elasticity $E_f$ [GPa] |
|---|---|---|
| 9 | 1475 | 56.3 |

*2.2.3. Steel reinforcement.* Shear, top and bottom (only in case of traditional RC beams) reinforcement was made of steel grade B500SP. Mechanical properties of this reinforcement are presented in Table 4.

**Table 4**. Mechanical properties of steel reinforcement.

| Characteristic yield strength $f_{yk}$ [MPa] | Characteristic tensile strength $f_{tk}$ [MPa] | Modulus of elasticity $E_s$ [GPa] |
|---|---|---|
| 500 | 575 | 205 |

### *2.3. FE model of the beams*

The finite element (FE) model of considered beams was implemented in ABAQUS environment [9]. The analysis was performed on 2D model and the following assumptions were adopted:

- concrete damage plasticity (CDP) model of concrete [10] was assumed,
- tension stiffening effect was taken into account,
- BFRP reinforcement was assumed as a linear elastic isotropic material,
- steel reinforcement was assumed as a linear elastic-plastic material with isotropic hardening,
- the reinforcement was modelled as two-node truss elements embedded in four-node elements of plane stress (Fig. 2).

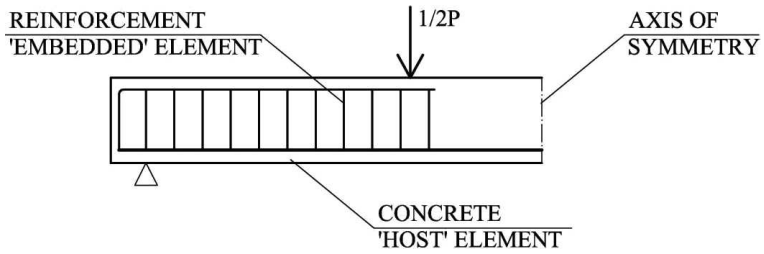


FIG. 2. Scheme of the 2D FE model.

The numerical model of the beams consisted of two different types of finite element:

- T2D2 – two-node 2D truss elements,
- CPS4R – four-node plane stress elements with reduced integration.

The concrete was modelled as concrete damage plasticity material, which was based on the brittle-plastic degradation model [11]. For concrete under uniaxial compression, the stress-strain curve shown in Fig. 3 was adopted [12].

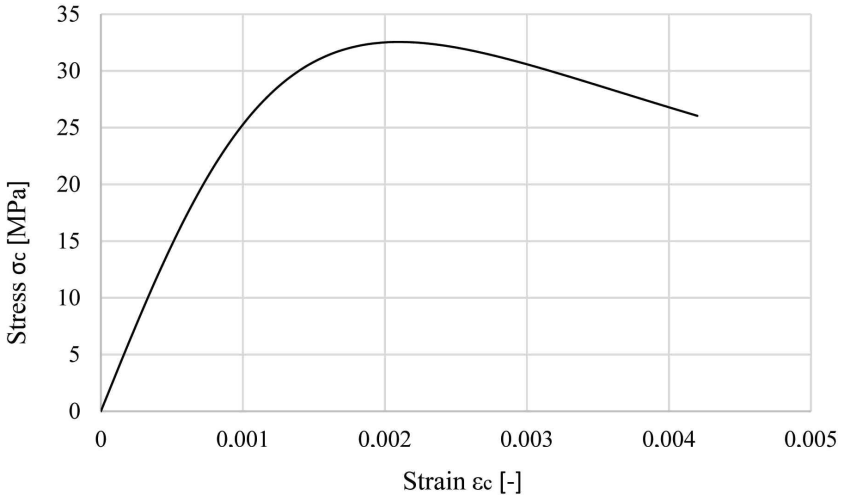


FIG. 3. Response of concrete to uniaxial loading in compression.

The tension stiffening effect was taken into account by applying a modified WANG and HSU [13] formula (Eq. (2.1)) to describe the behaviour of concrete under tension (Fig. 4):

$$\begin{aligned} &\sigma_t = E_c \varepsilon_t, \varepsilon_t \leq \varepsilon_{cr}, \\ &\sigma_t = f_{ctm} \left( \frac{\varepsilon_{cr}}{\varepsilon_t} \right)^n, \qquad \varepsilon_t > \varepsilon_{cr}, \end{aligned} \tag{2.1}$$

where $E_c$ is the modulus of elasticity of concrete, $\varepsilon_t$ is the tensile strain of concrete, $\varepsilon_{cr}$ is the tensile strain at concrete cracking, $f_{ctm}$ is the average tensile strength of concrete and $n$ is the rate of weakening.

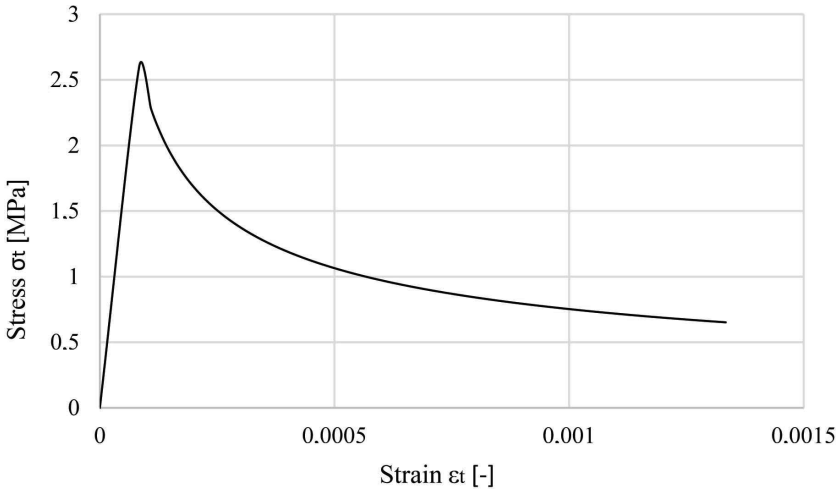


FIG. 4. Response of concrete to uniaxial loading in tension.

## 3. Numerical simulation results, data analysis and discussions

### *3.1. Failure mode and ultimate load*

Table 5 presents the numerical and theoretical [3, 7] ultimate loads for all considered beams. According to the results of FEM simulation all BFRP members failed in a brittle mode due to reinforcement rupture (B1) or concrete

**Table 5**. The numerical (FEM) and theoretical (ACI and EC2) ultimate loads.

| Beam designation | Reinforcement ratio $\rho_f$ [%] | Balanced reinforcement ratio $\rho_{fb}$ [%] | $P_u$ FEM [kN] | Failure mode* | $P_u$ ACI [kN] | $P_u$ EC2 [kN] |
|---|---|---|---|---|---|---|
| B1 | 0.15 | 0.16 | 30.2 | RR | 27.5 | 27.8 |
| B2 | 0.60 | | 61.2 | CC | 51.3 | 59.7 |
| B3 | 1.00 | | 76.8 | CC | 62.8 | 73.0 |
| B4 | 2.00 | | 102.8 | CC | 80.9 | 94.1 |
| B5 | 3.00 | | 114.8 | CC | 92.5 | 107.6 |
| B6 | 4.00 | | 119.8 | CC | 101.0 | 117.5 |

* CC – concrete crushing, RR – reinforcement rupture

crushing (B2–B6). It was assumed that the value of the maximum compressive concrete strain is about 0.0042 [14].

As can be observed in Table 5 and in Fig. 5, the reinforcement ratio has a significant influence on the flexural strength of BFRP beams. The increase of up to 3% in the reinforcement ratio results in an increase in the ultimate loads. This value is close to that found in the literature [14, 15]. Further rise in the reinforcement ratio does not result in a substantial increase in the flexural strength of the beams, thus the use of greater amount of reinforcement is not economically justified.

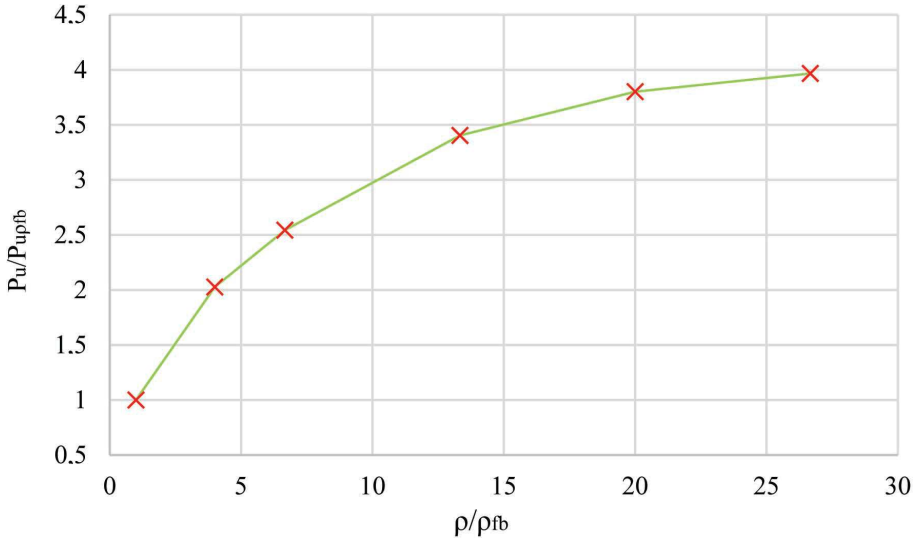


FIG. 5. Maximum ultimate load ratio $P_u/P_{u\rho fb}$ as a function of ratio $\rho/\rho_{fb}$.

As stated in ACI 440.1R-06 [3], the failure mode is governed by concrete crushing when the reinforcement ratio $\rho_f$ is greater than the balanced reinforcement ratio $\rho_{fb}$:

$$\rho_f = \frac{A_f}{bd}, \tag{3.1}$$

$$\rho_{fb} = 0.85\beta_1 \frac{f_c}{f_{fu}} \frac{E_f \varepsilon_{cu}}{E_f \varepsilon_{cu} + f_{fu}}, \tag{3.2}$$

where $A_f$ is the area of BFRP reinforcement, $b$ is the width of the section and $d$ is the effective depth. In Eq. (3.2), $\beta_1$ is the ratio of depth of equivalent rectangular stress block to depth of the neutral axis, $f_c$ is the concrete compressive strength, $f_{fu}$ is the design tensile strength of BFRP reinforcement, $E_f$ is the modulus of elasticity of FRP, and $\varepsilon_{cu}$ is the maximum concrete strain (0.003

for ACI 440.1R-06 [3]). The actual and balanced reinforcement ratios are compared in Table 5. Beams B2–B6 had higher reinforcement ratios than $\rho_{fb}$, hence according to code [3], failure by concrete crushing was expected in all of them. This mode of failure was confirmed by the numerical analysis.

As can be observed in Table 5, the flexural capacity calculated according to the codes [3, 7] is underestimated. Its value is lower than the one obtained from FEM analyses by about 10–27% and 2–9% for ACI and EC2, respectively. These differences may be caused by the value of the maximum concrete compressive strain $\varepsilon_{cu}$ which is assumed in these codes as 0.0030 for ACI and 0.0035 for EC2. The results of experiments in [14] show that the actual ultimate concrete strain $\varepsilon_{cu}$ is higher, and is equal to about 0.0042–0.0047.

### *3.2. Deflections*

Figure 6 shows numerical load-deflection curves for all the beams. It is clear from the graph that the reinforcement ratio has a considerable effect on the stiffness of the beams. As expected, deflections of these elements increase with a decrease in the reinforcement ratio.

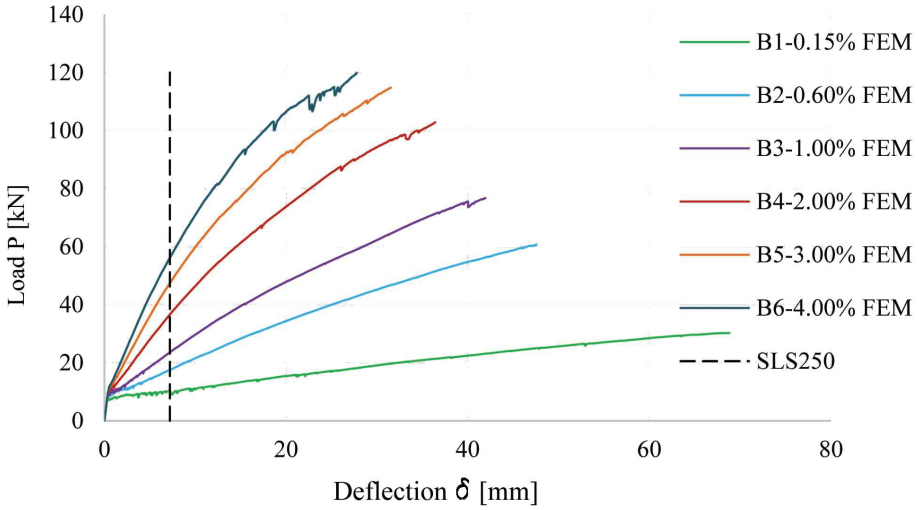


FIG. 6. Numerical load – midspan deflection curves (B1–B6 beams).

Table 6 presents deflections and span-to-deflection ratios for ultimate loads as well as service loads for permissible deflections (equal to about $L/250$) of the beams. For the ultimate loads, the value of the span-to-deflection ratio varied between 26 and 64. In comparison to the service deflection limit of $L/250$ this value was relatively low, thus the design of all the beams was governed by the serviceability limit state.

**Table 6**. Deflections and service loads.

| Beam designation | Ultimate load $P_u$ | | | Deflection $\delta = L/250$ | |
|---|---|---|---|---|---|
| | $P_u$ [kN] | $\delta_{\max}$ [mm] | $L/\delta_{\max}$ | $P_{L/250}$ [kN] | $P_{L/250}/P_u$ |
| B1 | 30.2 | 68 | 26 | 9.9 | 0.33 |
| B2 | 61.2 | 48 | 38 | 17.5 | 0.29 |
| B3 | 76.8 | 42 | 43 | 23.6 | 0.31 |
| B4 | 102.8 | 36 | 50 | 36.6 | 0.36 |
| B5 | 114.8 | 32 | 56 | 47.5 | 0.41 |
| B6 | 119.8 | 28 | 64 | 56.2 | 0.47 |

As can be observed in Table 6, service loads were about 29–47% of the limit loads for the considered beams. These values correspond well with the values obtained for RC elements with other types of FRP reinforcement [6, 14].

When comparing theoretical predictions obtained based on ACI (Eq. (3.3)) and EC2 (Eq. (3.4)) with the results of FE analyses (Fig. 7), it can be observed that up to the service load there is good agreement between numerical values of deflections and the ones calculated according to the codes [3, 7]. However, for higher loads both codes underestimate deflections. These differences can be connected with the fact that these theoretical approaches use a simplified linear stress-strain constitutive relationship for concrete

$$I_e = \left(\frac{M_{cr}}{M_a}\right)^3 \beta_d I_g + \left[1 - \left(\frac{M_{cr}}{M_a}\right)^3\right] I_{cr} \leq I_g. \tag{3.3}$$

Equation (3.3) shows the expression for an effective moment of inertia $I_e$ of the concrete section according to ACI, where $I_g$ is the gross moment of inertia of concrete section, $I_{cr}$ is the moment of inertia of the cracked section, $M_{cr}$ is the cracking moment, $M_a$ is the maximum moment in the member and $\beta_d$ is the reduction coefficient related to the reduced tension stiffening effect

$$\delta = \zeta \delta_{II} + (1 - \zeta)\delta_I. \tag{3.4}$$

Equation (3.4) shows the formulation for deflections $\delta$ according to Eurcode 2, where $\delta_I$ is an uncracked-state deflection, $\delta_{II}$ is a fully cracked-state deflection and $\xi$ is the coefficient related to the tension stiffening effect.

In case of steel RC beams (Fig. 8), values of deflections were about 60–70% less than deflections of non-metallic RC elements. These values are close to those found in the literature [16]. This is caused by the low value of moduli of elasticity of BFRP reinforcement.

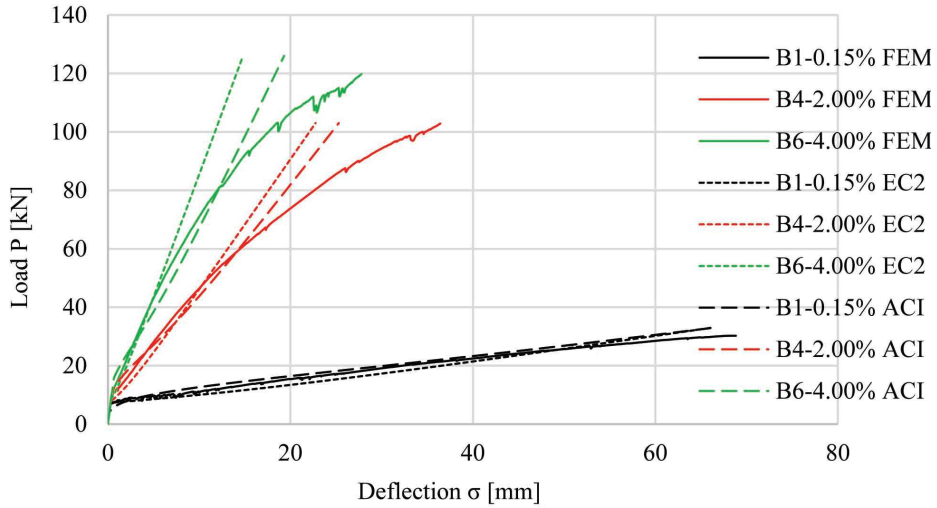


FIG. 7. Numerical and theoretical load – midspan deflection curves (B1, B4, B6 beams).

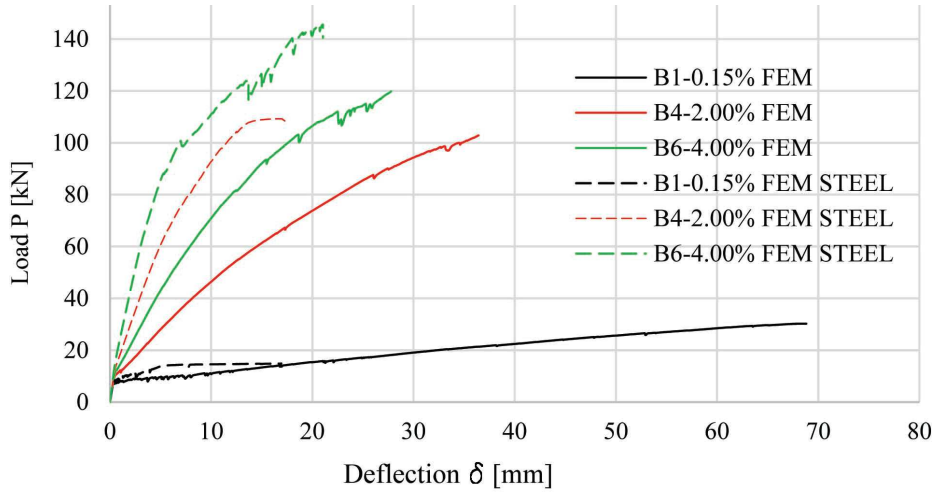


FIG. 8. Numerical load – midspan deflection curves for basalt (FEM) and steel (FEM STEEL) RC beams.

## 4. CONCLUSIONS

This paper presents the results of numerical and theoretical study of the flexural behaviour of BFRP RC beams. Based on these results, the following conclusions may be drawn:

- The reinforcement ratio has a significant effect on the flexural behaviour of BFRP RC beams. The increase of up to about 3% in the reinforcement ratio results in an increase in the ultimate loads. Further rise in the reinforcement ratio does not result in a substantial increase in the flexural strength of the beams.
- The failure mode is governed by concrete crushing when the reinforcement ratio $\rho_f$ is greater than the balanced reinforcement ratio $\rho_{fb}$ (according to ACI 440.1R-06). All beams behave almost linearly up to the moment of failure, which takes place at relatively large deflections.
- At the service load level, the deflections calculated according to ACI 440.1R-06 and EC2 are in close agreement with the results of the FE analysis. For higher loads these codes underestimate deflections.
- The ultimate loads, calculated according to ACI 440.1R-06 and Eurocode 2, are underestimated. This underestimation may be caused by the value of the ultimate concrete strain $\varepsilon_{cu}$ which is assumed in these codes, and it is lower than the value of $\varepsilon_{cu}$ obtained in the experiments.
- Deflections in steel RC beams are about 60–70% less than in case of BFRP RC elements with the same reinforcement ratio.
- Design of BFRP RC beams is governed by the serviceability limit states.

## Acknowledgment

The numerical simulations were partially supported by the Ministry of Science and Higher Education under doctoral grant 01/11/DSMK/0291.

## References

1. Pawłowski D., Szumigała M., *Use of FRP reinforcement in building constructions* [in Polish], Przegląd Budowlany, **3**: 47–50, 2014.
2. *FRP reinforcement in RC structures, technical report*, fib Bulletin, International Federation for Structural Concrete (fib), **40**: 3–30, 2007.
3. ACI 440.1R-06, *Guide for the design and construction of structural concrete reinforced with FRP bars*, ACI Committee 440, 2006.
4. http://www.polprek.pl/pdf/POLPREK-Badania-wytrzymalosc.pdf, 2014.
5. Nanni A., *North American design guidelines for concrete reinforcement and strengthening using FRP: principals, applications and unresolved issues*, Construction and Building Materials, **17**(6–7): 439–446, 2003.
6. Barris C., Torres L., Comas J., Miàs C., *Cracking and deflections in GFRP RC beams: an experimental study*, Composites: Part B, **55**: 580–590, 2013.
7. EN 1992-1-1:2003, *Eurocode 2: Design of concrete structures – Part 1-1: General rules and rules for buildings*, Technical Committee CEN/TC250, 2004.

8. EN 206:2013, *Concrete. Specification, performance, production and conformity*, Technical Committee CEN/TC 104, 2013.

9. ABAQUS, *Abaqus Analysis User's Manual*, Version 6.10, Dassault Systems, 2010.

10. Lubliner J., Oliver J., Oller S., Onate E., *A Plastic-damage model for concrete*, International Journal of Solids Mechanics, **25**(3): 299–326, 1989.

11. Lee J., Fenves G.L., *Plastic-damage model for cyclic loading of concrete structures*, Journal of Engineering Mechanics, **124**(8): 892–900, 1998.

12. Saenz L.P., *Discussion of paper "Equation for stress-strain curve of concrete" by Desai P. and Krishnan S.*, Journal of American Concrete Institute, **61**: 1229–1235, 1964.

13. Wang T., Hsu T.T.C., *Nonlinear finite element analysis of concrete structures using new constitutive models*, Computers and Structures, **79**(32): 2781–2791, 2001.

14. Barris C., Torres L., Tauron A., Baena M., Catalan A., *An experimental study of the flexural behaviour of GFRP RC beams and comparison with prediction models*, Composites Structures, **91**(3): 586–295, 2009.

15. Mousavi S., Esfahani M., *Effective moment of inertia prediction of FRP-reinforced concrete beams based on experimental results*, Journal of Composites for Construction, **16**(5): 490–498, 2012.

16. Garbacz A., Łapko A., Urbański M., *Investigation on concrete beams reinforced with basalt rebars as an effective alternative of conventional R/C structures*, Procedia Engineering, **57**: 1183–1191, 2013.

*Received July 12, 2014; accepted version January 18, 2016.*